LEARNING EFFICIENT HYBRID PARTICLE-CONTINUUM REPRESENTATIONS OF NON-EQUILIBRIUM N-BODY SYSTEMS

Anonymous authors
Paper under double-blind review

ABSTRACT

An important class of multi-scale, non-equilibrium, N-body physical systems deals with an interplay between particle and continuum phenomena. These include hypersonic flow and plasma dynamics, materials science, and astrophysics. Hybrid solvers that combine particle and continuum representations could provide an efficient framework to model these systems. However, the coupling between these two representations has been a key challenge, which is often limited to inaccurate or incomplete prescriptions. In this work, we introduce a method for Learning Hybrid Particle-Continuum (LHPC) models from the data of first-principles particle simulations. LHPC analyzes the local velocity-space particle distribution function and separates it into near-equilibrium (thermal) and far-from-equilibrium (non-thermal) components. The most computationally-intensive particle solver is used to advance the non-thermal particles, whereas a neural network solver is used to efficiently advance the thermal component using a continuum representation. Most importantly, an additional neural network learns the particle-continuum coupling: the dynamical exchange of mass, momentum, and energy between the particle and continuum representations. Training of the different neural network components is done in an integrated manner to ensure global consistency and stability of the LHPC model. We demonstrate our method in an intense laser-plasma interaction problem involving highly nonlinear, far-from-equilibrium dynamics associated with the coupling between electromagnetic fields and multiple particle species. More efficient modeling of these interactions is critical for the design and optimization of compact accelerators for material science and medical applications. Our method achieves an important balance between accuracy and speed: LHPC is $8\times$ faster than a classical particle solver and achieves up to 6.8-fold reduction of long-term prediction error for key quantities of interest compared to deep-learning baselines using uniform representations.

1 INTRODUCTION

The dynamics of physical systems is often nonlinear and involves the competition of different processes across a wide range of spatial and temporal scales. This gives rise to local non-equilibrium conditions (in the thermodynamic sense) that results in the failure of common numerical approaches. While continuum models (*e.g.*, based on fluid equations) can provide accurate and computationally efficient descriptions of near-equilibrium systems at large scales, they break down when significant departures from local equilibrium are encountered (often at small scales) and give rise to important N-body phenomena. Kinetic (*e.g.*, particle-based) numerical methods can accurately describe these non-equilibrium phenomena but are very computationally intensive, limiting their practical application to small scales. Over the last decades, this has motivated efforts to develop hybrid algorithms that can more efficiently couple continuum and particle representations in a variety of fields, including hypersonic gas dynamics (Schwartzentruber & Boyd, 2006), high-energy-density physics (Fiuza et al., 2011), and plasma physics (Bai et al., 2015).

Plasmas — hot ionized gases of charged particles — are a particularly challenging class of complex physics systems, where long-range electromagnetic interactions inevitably drive multi-scale and far-from-equilibrium dynamics. Indeed, plasma research associated with controlled nuclear

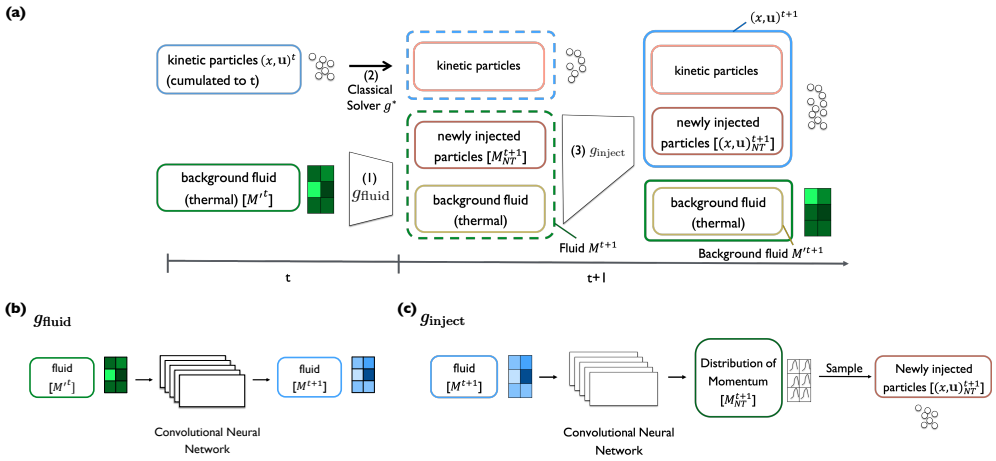

Figure 1: (a) Schematic of our LHPC architecture. It consists of three components: (1) a neural network g_{fluid} for evolution of thermal sub-population with fluid representation; (2) a solver g^* for the evolution of the non-thermal energetic sub-population with particle representation; (3) neural networks that model the injection of particles from fluid state (g_{inject}). (b) and (c) illustrate the architectures of the components (1) and (3).

fusion, advanced laser-plasma particle accelerators, and most space and high-energy astrophysical environments have long stimulated the development of hybrid particle-continuum representations to accurately and efficiently capture the nonlinear dynamics of these systems. In all these cases, small-scale kinetic processes can accelerate a very small group of particles to energies significantly above the mean (thermal) energy, driving the system out of equilibrium. Importantly, this small group (few %) of non-thermal particles can carry away a large fraction (up to 50%) of the system energy and thus impact its global evolution. This motivated the recent development of hybrid representations that use a fluid solver to model the near-equilibrium (thermal) part of the particle distribution and a particle-based kinetic solver to model the evolution of high-energy particles (Kowal et al., 2011; Bai et al., 2015; Guidoni et al., 2016). However, the coupling of the two representations has been based on over-simplified phenomenological prescriptions that can limit their validity and applicability.

In this work, we introduce a method for Learning Hybrid Particle-Continuum (LHPC) models to address the key challenge of efficiently and accurately coupling fluid and kinetic representations of far-from-equilibrium N-body systems. LHPC combines a classical particle-in-cell (PIC) solver to advance the non-thermal particle distribution with a neural network surrogate model that efficiently advances the thermal component using a continuum representation. Most importantly, our key contribution is the use of an additional neural network to learn the self-consistent particle-continuum coupling: the dynamical exchange of mass, momentum, and energy between the particle and continuum representations. This coupling is learned from the data of first-principles PIC simulations, providing an accurate and physics-informed description that addresses the main limitation of previous hybrid methods.

While the combination of classical numerical solvers and deep learning has been explored before (Um et al., 2020; Vlachas et al., 2022), these have been primarily based on uniform representations. The use of machine learning techniques to learn efficient and accurate coupling between continuum and particle representations introduced in this work is a promising and important route for addressing the multi-scale and multi-physics challenge of modeling N-body non-equilibrium systems.

We demonstrate our method on a challenging non-linear, far-from-equilibrium N-body system: the interaction of an intense laser with a solid-density plasma and resulting particle acceleration. Present-day high-power lasers reach intensities in excess of 10^{20}W/cm^2, which nearly instantaneously vaporize and ionize solid-state matter upon interaction, resulting in high-energy-density plasma. These interactions give rise to nonlinear and kinetic processes that establish strong electric fields in the plasma and accelerate particles to high energies over very compact distances. In the last two decades, there has been great interest in exploiting these laser-plasma based accelera-

tors for a wide range of applications, including material science (Patel et al., 2003), imaging (Rygg et al., 2008), and medical therapy (Kroll et al., 2022). Due to the need to capture detailed kinetic physics associated with these interactions, numerical modeling has relied primarily on fully kinetic PIC simulations, which are too computationally intensive – in fact, one-to-one modeling of experimental systems is computationally prohibitive even on the largest supercomputers. Effective hybrid particle-continuum representations have not been previously established for this problem. This is thus a prime example for testing our model and evaluating the ability of LHPC to learn efficient and accurate hybrid representations that can have a transformative impact in the modeling of these complex laser-plasma interactions.

Our results show that LHPC achieves an important balance between accuracy and speed: LHPC is 8 times faster than a classical particle solver, and achieves up to 6.8-fold reduction of long-term prediction error for key quantities of interest when compared to deep-learning baselines using uniform representations. This opens up a novel route to develop more efficient and accurate particle-continuum descriptions across different domains involving non-equilibrium N-body systems, and represents a key step for data-driven multi-scale algorithms for nonlinear physical systems.

2 Related Works

Deep learning has recently emerged as a powerful tool to complement Um et al. (2020) or serve as a surrogate for classical solvers (Sanchez-Gonzalez et al., 2020). They accelerate simulation of physical systems through larger spatial resolution (Um et al., 2020; Kochkov et al., 2021) or temporal intervals (Li et al., 2021), explicit forward method (Tang et al., 2020; Wu et al., 2022b), or via reduced representations (Sanchez-Gonzalez et al., 2020; Wu et al., 2022a). However, almost all works employ a uniform representation, either all particles or all fluid, without considering the multi-scale characteristics present in many physical systems. One important exception is LED (Vlachas et al., 2022), which performs hybrid evolution in the temporal dimension. Specifically, they employ a solver to simulate the full system in some interval of time and use latent evolution to evolve in other parts of time, with a pre-defined alternative schedule. In comparison, our work addresses the multi-scale, multi-physics modeling of dynamical physical systems from a different perspective: it aims to learn an accurate and efficient coupling between different representations involving different physical processes and scales, namely a hybrid particle-continuum representation which is critical to describe non-equilibrium N-body systems. To the best of our knowledge, machine learning methods have not yet been used to address this problem.

3 Problem setup and preliminaries

Task setup. In general, simulations of the time-evolution of a dynamical system can be described as follows. The state of the system at time t is s^t, and there exists a ground-truth evolution g^* that evolves this state:

$$s^{t+1} = g^*(s^t),\ t = 0, 1, 2, \ldots \tag{1}$$

The ground-truth evolution g^* can either be the physical world which is challenging to predict, or a first-principles numerical solver which can be slow and expensive for large-scale systems. Assume that we have a pre-defined mapping h which maps the state s^t to a representation S^t: $S^t = h(s^t)$, $t = 0, 1, 2, \ldots$, such that S^t captures the essence of the system. For example, consider an original state s^t represented by particles, and S^t a fluid representation which describes the system with statistics of the particles within each cell (see below). Alternatively, h may be an identity mapping resulting in $S^t = s^t$. A hybrid h mapping will apply both of these representations to different groups of particles. Given the states $\{s^t\}, t = 1, 2, \ldots, T$, the task is to design a proper representation $S^t = h(s^t)$, and learn a surrogate model g_θ, typically in terms of a neural network, which approximates the ground truth evolution of S^t:

$$\hat{S}^{t+1} = g_\theta(S^t),\ t = 0, 1, 2, \ldots \tag{2}$$

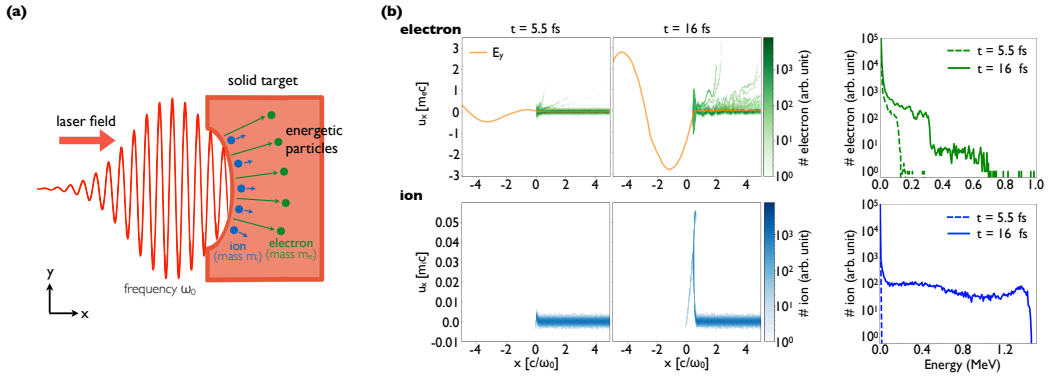

Figure 2: (a) Intense laser-plasma interactions generate energetic particles with rich dynamics. (b) Projection of the particle dynamics onto the longitudinal momentum (u_x)-position (x) phase spaces, the laser E-field (orange), and the corresponding energy spectra of the particles at two different times.

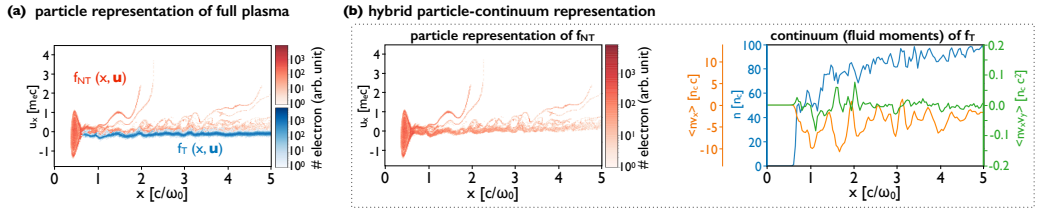

Figure 3: Representations of plasma illustrated with electrons. (a) Particle representation of the non-thermal (f_{NT}) and thermal (f_{T}) populations. (b) Hybrid particle-continuum representation showing the same particle representation of f_{NT} and example velocity moments of the thermal electron fluid.

Here $\hat{S}^{t+1}$ is the model g_θ's prediction of S^{t+1}. Our goal is to have the long-term autoregressive evolution of the learned surrogate model $\hat{S}^{t+k} = g_\theta \circ ... \circ g_\theta(S^t)$ (composing k times) to closely match the ground-truth S^{t+k}.

Physical problem overview. In this work, we consider the interactions of intense laser pulses with plasmas, where the laser field accelerates the plasma electrons near the front surface, which in turn sets up a charge separation, generating electric (E-) and magnetic (B-) fields that accelerate and deflect the ions (Fig. 2; see Appendix A for details). These interactions of the charged particles with E- and B-fields (collectively EM-field) occur on ultra-fast time scales ($\sim 10^{-15}$ s), and can produce electrons and ions with energies exceeding 10^6 electronvolt ($\equiv 1$ MeV) – with the electrons moving at close to the speed of light c. These are prime examples of non-equilibrium systems, for which computationally expensive first-principles simulations are necessary to accurately capture the associated non-linear dynamics.

Particle and continuum representations. The two dominant representations of the plasma system considered in our work are particle (kinetic) and continuum (fluid) representations. A particle representation $\{(x_i^t, \mathbf{u}_i^t, Q_i)\}$ describes the position x_i^t, momentum vector $\mathbf{u}_i^t$, and other static properties Q_i (*e.g.*, mass or charge) of each particle i. The particles interact with each other, and change their position and momentum accordingly. In contrast, a fluid representation M^t is defined on a fixed grid or mesh. The values on each vertex represent the moments (statistical averages) of the momenta of the particles residing around the vertex. These statistical quantities summarize the states of a large number of particles, permitting a more compact representation. Their physical meaning is well established. For example, the first three moments correspond to the fluid observables mass density, fluid velocity, and pressure. We note that in general an exact representation of the full particle distribution requires an infinite number of fluid moments (see Appendix A.1). However, if the particle distribution is near local thermodynamic equilibrium it can be described by a compact set of fluid moments. A hybrid particle-continuum model aims to provide an efficient description of a

more general distribution of particles by coupling a particle representation for far-from-equilibrium particles with a continuum representation for particles near equilibrium.

Thermal and non-thermal population. In this context, we refer to the group of particles in a near equilibrium state as *thermal*, for which the momentum distribution can be well described by a Gaussian (*i.e.* requiring only the mean and variance). On the other hand, we refer to the particles that are far from equilibrium as *non-thermal*. These are the outliers from this Gaussian distribution. In terms of the total particle distribution function, f, this allows us to decompose it into a *thermal*, f_{T}, and *non-thermal*, f_{NT} components, with $f = f_{\mathrm{T}} + f_{\mathrm{NT}}$. See Fig. 3 for an illustration of this separation in physical problem of intense laser-plasma interactions considered in this work; details of the separation algorithm are presented in Appendix B.

4 METHOD

4.1 METHOD OVERVIEW

Here we introduce Learning Hybrid Particle-Continuum Models (LHPC) to address the key challenges in hybrid representations of non-equilibrium dynamical systems. Specifically LHPC learns two key components, for the evolution of the fluid, and coupling between the particle and fluid representations. In Figs. 1, 3 and the following sections, we detail the data generation and preparation procedure, the main architecture, and its application to the study of intense laser-plasma interactions.

4.1.1 DATA GENERATION AND PREPARATION FROM FIRST-PRINCIPLES SIMULATIONS

Although computationally expensive, full PIC simulations provide ground truth data from first-principles particle-based evolution of plasma dynamics. We run full PIC simulations of laser-plasma interactions in a one spatial dimension, three velocity dimension (1D3V) setting, where the laser intensity is varied to generate multiple trajectories. A trajectory is composed of a simulation with 2000 time steps of evolution, involving 1.5 million (numerical) particles evolving on a $\simeq$10k-cell grid, and is 200 GB in size (see Appendix A.3 for details).

To train the two learned components of LHPC, we transform the ground truth particle data into the fluid and particle representations at each time step. This is achieved by first applying an algorithm that separates the particles into thermal and non-thermal populations (*e.g.* Fig. 3; for details see Appendix B). The labeled particle data is then transformed, with the non-thermal population keeping the original particle representation, and using the velocity moments (up to 2nd order) to represent the thermal fluid. As the system evolves, a small fraction of the particles from the thermal population will gain a significant amount of energy to get detached from the thermal distribution, becoming non-thermal. They are said to be "injected" into the non-thermal population. The transformed ground truth data therefore provides the information of the evolution of both representations, and the coupling (injection) between them.

4.1.2 ARCHITECTURE

LHPC evolves the system state S^t at time t to state S^{t+1} at time $t+1$ with three components (Fig. 1):

(1) A neural network $g_{\text{fluid},\theta}$ with parameters θ which evolves the (thermal) fluid (Fig. 1b).

(2) A ground-truth solver g^* which evolves the non-thermal particles.

(3) A neural network $g_{\text{inject},\varphi}$ with parameters φ which models the interplay of the fluid and particle populations (Fig. 1c). In particular, it models the injection of new non-thermal particles from the fluid, and updates the existing fluid and particle populations accordingly.

At inference, these processes are iterated autoregressively to predict the state of the system into the long-term future.

4.2 LHPC FOR LASER-PLASMA INTERACTIONS

Here, we employ LHPC to model laser-plasma simulations. The space in x is divided into C consecutive cells: $c \in [c_{\text{left}}, c_{\text{left}+1}, \ldots, c_{\text{right}}]$ in the x direction. The state S^t consists of:

$$S^t := ((M^t, {M'}^t, {M_{\text{NT}}}^t), ({x_{\text{NT}}}^t, {\mathbf{u}_{\text{NT}}}^t, {x_{\text{PIC}}}^t, {\mathbf{u}_{\text{PIC}}}^t), (E^t, B^t))_c : \\ c \in [c_l, c_{l+1}, \ldots, c_r]$$

where the velocity moments of different populations M and the non-thermal particles $(x, \mathbf{u})$ interact through the fields (E, B). The full pipeline in Fig. 8 in Appendix C further visualizes the dependencies amongst these components and documents what each quantity represents. The following sequence of operations is used to evolve the system from time t to time $t+1$:

$$M^{t+1} \leftarrow g_{M,\theta}((E,B)^t, {M'}^t)$$
Advance fluid moments according to electromagnetic (EM-) field on the grid. (1a)
$g_{M,\theta}$ is an instantiation of the $g_{\text{fluid},\theta}$ introduced in Sec. 4.1.2.

$$M_{\text{NT}}^{t+1} \leftarrow g_{M_{\text{NT}},\varphi}(M^{t+1}, {M'}^t)$$
Compute moments of new non-thermal particles to be injected (1b)
$g_{M_{\text{NT}},\varphi}$ is an instantiation of the $g_{\text{inject},\varphi}$ introduced in Sec. 4.1.2.

$$(x, \mathbf{u})_{\text{NT}}^{t+1} \leftarrow \mathcal{N}(M_{\text{NT}}^{t+1})$$
Inject new non-thermal particles by sampling from distribution with M_{NT}^{t+1} (1c)

$${M'}^{t+1} \leftarrow (x_{\text{NT}}, \mathbf{u}_{\text{NT}}, M)^{t+1}$$
Update fluid moments to conserve mass, momentum, and energy (1d)

$$(x, \mathbf{u})_{\text{PIC}}^{t+1} \leftarrow \left[G((x, \mathbf{u})_{\text{PIC}}^t, (E,B)^t); \quad (x, \mathbf{u})_{\text{NT}}^{t+1}\right]$$
Advance existing particles and append newly injected non-thermal particles (1e)

$$J^{t+1} \leftarrow (M', x, \mathbf{u})^{t+1}$$
Deposition of electric current J from particles and fluid to grid (1f)

$$(E,B)^{t+1} \leftarrow J^{t+1}$$
Advance EM-field on the grid using Maxwell's equations (1g)

The operators $g_{M,\theta}$ and $g_{M_{\text{NT}},\varphi}$ are instantiated from $g_{\text{fluid},\theta}$ and $g_{\text{inject},\varphi}$ and are deep neural network models learned from data. The operator G and the field solver advances the non-thermal particles with the classical PIC solver. A more detailed description of each component a–g can be found in Appendix C.1.

4.2.1 Baselines

We compare with state-of-the-art deep learning-based surrogate model of Fourier Neural Operator (FNO; Li et al. 2021), and a baseline CNN that has the same architecture as our fluid evolution model without hybrid representation. Both architectures are evaluated on two representations: (1) an all fluid representation which models all particles as fluid defined on each cell; (2) a bi-Gaussian fluid representation, that models the more static thermal particles and the more dynamic non-thermal particles each as a Gaussian.

We compare the hybrid pipeline with naive baseline (1), which treats the entire system as a fluid and advances the system by learning g as:

$$M^{t+1}, (E,B)^{t+1} = g((E,B)^t, M^t).$$

We also compare with an improved "bi-fluid" baseline that models the thermal population and the non-thermal particles each as a Gaussian, and advances the system by learning g as:

$$M^{t+1}, M_{\text{PIC}}^{t+1}, (E,B)^{t+1} = g((E,B)^t, M^t, M_{\text{PIC}}^t).$$

We care especially about the error on the moments of the non-thermal subpopulation M_{PIC} to understand how the respective methods model the most dynamic subpopulation of particles.

5 EXPERIMENTS

In this section, we aim to answer two questions: (1) does our LHPC model with hybrid representation achieve better accuracy than learning the evolution with a pure fluid representation? (2) Does LHPC offer speedup, compared to the full-PIC solver that evolves the full system in first principles with particle representation? We evaluate LHPC and baselines in the N-body laser-plasma interactions system described above. We evaluate both single-step prediction error and auto-regressive rollout error over 50 steps, where the state of the system changes significantly. We use relative L2 as the error metric – the ratio between L2 norm of error over L2 norm of ground-truth values.

5.1 DATA AND EXPERIMENT

Both the baseline and main pipeline are trained over 9 trajectories of PIC simulation. 10 trajectories were generated that vary over the normalized laser intensity a_0 from $[2, 4, \ldots, 20]$ and trajectory 5 ($a_0 = 10$) is held-out for testing (see Appendix A for details). In this way, we test the generalization of the models to novel initial conditions and environment setup. Each dataset consists of $T = 1500$ time steps and uses the separation strategy (details in Appendix B). For the nine datasets, we train with single-step loss on the time-range [0,1400], and validate on [1400, 1500]. We iterate on hyperparameters to obtain the best individual settings for both the baseline and hybrid pipelines respectively (detailed in Appendix). Then, the best models are finetuned using the multi-step loss with data from timeranges $[980, 1000] \cup [1080, 1100] \cup [1180, 1200] \cup [1280, 1300] \cup [1380, 1400]$, and validated on [1400, 1500]. We report the confidence intervals of the 1-, 20- and 50-step relative L2 errors on the held-out dataset and report the results in Table 1, which shows the error for the EM-field, the non-thermal particles (M_{PIC}) and the full fluid, respectively. Runtime for ground-truth (GT) solver and the compared models are also provided in Table 1. We provide additional results in Appendix D with an ablation study on trajectory 10 with the most intense laser ($a_0 = 20$).

5.2 RESULTS

Error comparison. From Table 1, we see that our LHPC typically outperforms the baselines in terms of error by a wide margin. Among the three aspects we evaluate, the EM-field error and the non-thermal particles (M_{PIC}) are the most important, since the EM-field is most sensitive to the local particle dynamics, and the non-thermal particles are typically the most important observable/deliverable of laser-plasma accelerators. An all-fluid description can be very efficient and accurate at describing the thermal (M) population, as is common for traditional fluid solvers. However, it fails to capture non-thermal particle acceleration, manifested in large errors for the field evolution (Field) and non-thermal population (M_{PIC}). Specifically, for Field, our LHPC achieves an error reduction of 91.0%, 91.3% and 85.4% (6.8-fold) for 1-, 20- and 50-step autoregressive rollout, compared to the best models among the baselines. Similarly, in the evaluation of M_{PIC}, our LHPC achieves an error reduction of 63.5%, 36.2%, 25.8% for 1-, 20- and 50-step predictions, respectively, demonstrating the ability of our LHPC to model accurately the dynamics of those energetic non-thermal particles. The Baseline CNN, although having the same architecture as our LHPC, cannot model accurately the non-thermal particles via either all-fluid or Bi-Gaussian representations, thus achieving much larger error. Specifically, while the use of a separate fluid description for the non-thermal population (Bi-Gaussian model) can help capture its impact on the system evolution, it still leads to significantly larger errors in the field evolution when compared to the LHPC model and cannot be used to fully describe the complex distribution of the non-thermal particles (see also Sec. 5.3). Comparing baseline and state-of-the-art FNO, we find that FNO performs comparable or slightly worse than Baseline CNN, likely due to the simpler architecture of CNN being more appropriate to capture the local fluid evolution. On predicting the fluid moments (M), our LHPC model performs comparably to Baseline that has the same CNN architecture, showing both models can model reasonably the dynamics of the fluid.

Method	Component	Error @ step 1	Error @ step 20	Error @ step 50	Speed (s/step)
GT Solver (full PIC)	–	–	–	–	9.21E-01
FNO: All-fluid	Field	5.77E-02 ± 1.52E-02	9.36E-01 ± 2.00E-01	2.57E+00 ± 8.56E-01	7.79E-02
	M_{PIC}	–	–	–	
	M	5.53E-03 ± 1.16E-03	6.79E-02 ± 1.47E-02	3.07E-01 ± 6.71E-02	
FNO: Bi-Gaussian	Field	2.98E-02 ± 2.36E-03	4.69E-01 ± 5.49E-02	9.65E-01 ± 1.51E-01	1.66E-01
	M_{PIC}	3.25E-02 ± 8.10E-03	3.83E-01 ± 9.30E-02	1.03E+00 ± 4.75E-01	
	M	6.92E-03 ± 1.17E-03	8.63E-02 ± 1.01E-02	2.38E-01 ± 3.45E-02	
Baseline: All-fluid	Field	1.97E-02 ± 7.53E-03	1.83E-01 ± 5.86E-02	7.16E-01 ± 3.66E-01	**4.61E-02**
	M_{PIC}	–	–	–	
	M	2.62E-03 ± 4.63E-04	**4.86E-02** ± 9.02E-03	**1.31E-01** ± 3.55E-02	
Baseline: Bi-Gaussian	Field	1.12E-02 ± 3.68E-03	1.31E-01 ± 2.61E-02	3.67E-01 ± 4.77E-02	1.10E-01
	M_{PIC}	2.24E-02 ± 9.21E-03	1.82E-01 ± 7.70E-02	5.00E-01 ± 8.01E-02	
	M	1.12E-02 ± 5.05E-04	6.07E-02 ± 8.69E-03	1.39E-01 ± 1.08E-02	
LHPC	Field	**1.01E-03** ± 1.57E-04	**1.14E-02** ± 6.76E-04	**5.34E-02** ± 6.68E-03	1.15E-01
	M_{PIC}	**8.18E-03** ± 2.02E-03	**1.16E-01** ± 6.69E-02	**3.71E-01** ± 7.83E-02	
	M	**4.51E-03** ± 7.12E-04	7.44E-02 ± 8.80E-03	1.80E-01 ± 2.88E-02	

Table 1: Results for the N-body laser-plasma interactions system on the held-out dataset. We evaluate three aspects of prediction: EM-field (Field), non-thermal particles (M_{PIC}), and the fluid moments M. Mean and 90% confidence interval are reported. The results are average performance on the held-out dataset over 15 independent rollouts with initial conditions at $t = 0, 100, \ldots, 1400$. Our LHPC achieves significant improvement on the EM-field predictions in both short- and long-terms. In terms of EM-field, LHPC achieves a 91.0%, 91.3%, and 85.4% (6.8-fold) reduction of error for 1-, 20- and 50-step rollouts, respectively, compared to the best-performing baseline. Similarly, for M_{PIC} LHPC achieves error reduction of 63.5%, 36.2%, 25.8% for 1-, 20- and 50-step predictions. Note that the performance is N/A for all-fluid representation models for M_{PIC} as they cannot model the non-thermal particles separately. For M prediction, our LHPC has comparable performance with the baselines, since both use similar architectures to model the thermal part of the distribution as fluid, but the baselines also receive M as an input whereas LHPC does not.

Runtime comparison. While achieving significant error reduction on predicting the EM-field and the non-thermal particles, our LHPC also achieves significant speedup compared to the Ground-truth (GT) full PIC solver, with a reduction of runtime by 8.0-fold. We also see that the runtime of LHPC is not much higher than full deep learning based baselines, showing that although our LHPC involves a GT solver to evolve the non-thermal particles, the increase in runtime is negligible since the non-thermal particles only constitute a small fraction of the system.

5.3 Visualization of Results

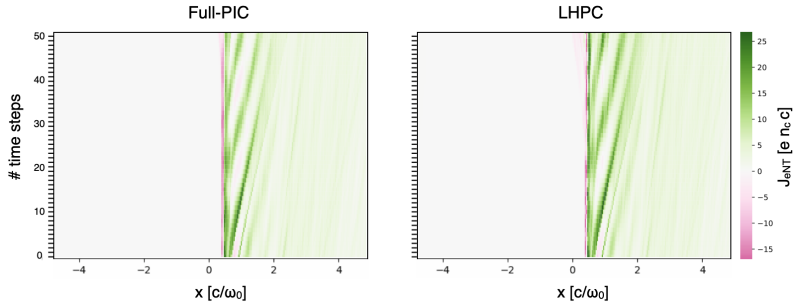

Figure 4: Comparison of the evolution of non-thermal electron current J_{eNT} between ground truth (Full-PIC) and LHPC across 50 steps of rollout.

In this section, we visualize the predictions of LHPC. An accurate evolution of the system dynamics relies on the correct EM-field (Eq. 1g), which is dictated by the electric current J (Eq. 1f). Figure 4 shows that our model can predict the evolution of J contribution from the non-thermal population accurately over 50 time steps of rollout. This is further illustrated in Fig. 5, where for the different contributions of J, good agreement between the predictions of our model and the ground truth is observed. Similarly, our model predictions for components of the E-field and the thermal fluid density

match well the ground truth after 20 steps of rollout. These results demonstrate faithful evolution of the important quantities that describe the dynamics of the fluid, the non-thermal particles, and the coupling between them. Importantly, our model is able to accurately capture the critical aspect of laser-plasma interactions — non-thermal particle acceleration (Fig. 6). Note that the highly non-trivial energy distribution of the accelerated (non-thermal) particles cannot be properly described with a few fluid moments and must rely on the accurate evolution of the particle representation.

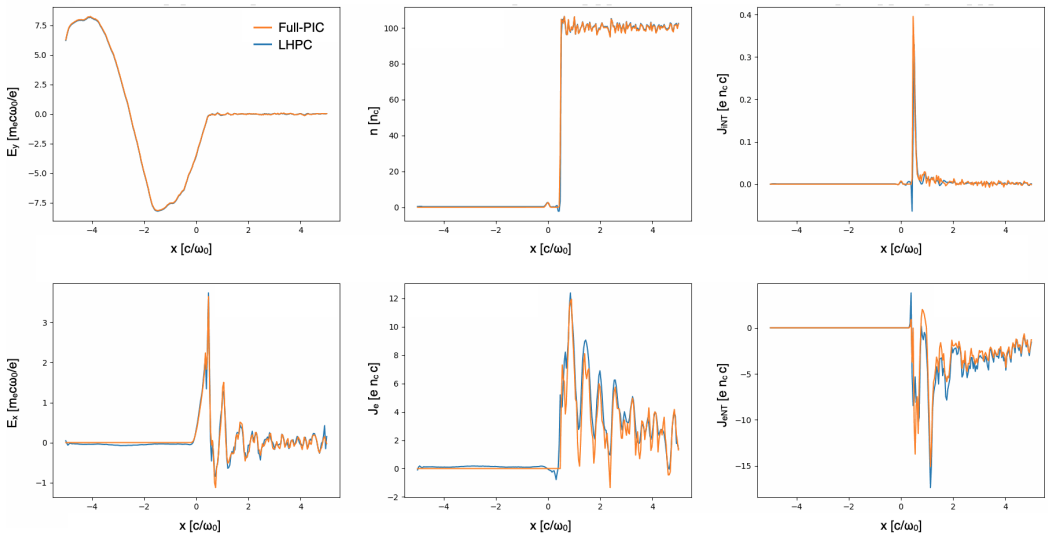

Figure 5: Comparison of ground truth (Full-PIC) and LHPC model predictions after 20 steps of rollout, for E-field components (left column) E_x, E_y, (middle) total density of the fluid n, and J contribution from the fluid electrons J_{e}, (right) non-thermal ions J_{iNT} and electrons J_{eNT}.

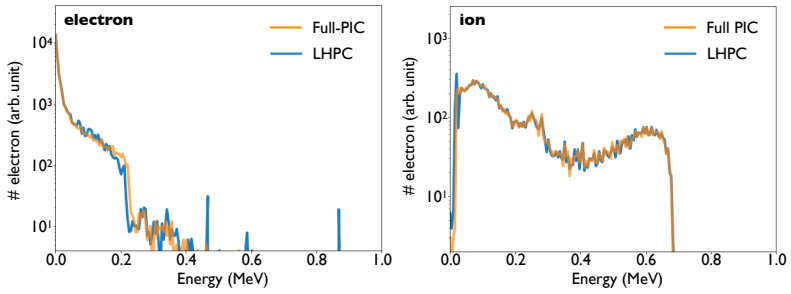

Figure 6: Comparison of energy spectrum of non-thermal electrons (left) and ions (right) between ground truth (Full-PIC) and LHPC after 20 steps of rollout.

6 Discussion and Conclusion

This work helps address a key challenge in modeling multi-scale, non-equilibrium, N-body systems by providing a novel hybrid particle-continuum model, whose coupling is learned from the data of first-principles simulations. LHPC outperforms the classical first-principles solver by an order of magnitude in speed, and the baseline method that models the entire system as a fluid by up to an order of magnitude in accuracy. Further speed-ups are expected in multiple dimensions as the non-thermal population constitutes a much smaller fraction of the system representation (see Appendix A.4).

Our method is generalizable towards finding more efficient and accurate particle-continuum descriptions across different domains involving non-equilibrium N-body systems, and represent a key step towards the development of advanced data-driven algorithms for multi-scale modeling of nonlinear physical systems.

REFERENCES

Xue-Ning Bai, Damiano Caprioli, Lorenzo Sironi, and Anatoly Spitkovsky. MAGNETOHYDRODYNAMIC-PARTICLE-IN-CELL METHOD FOR COUPLING COSMIC RAYS WITH A THERMAL PLASMA: APPLICATION TO NON-RELATIVISTIC SHOCKS. *The Astrophysical Journal*, 809(1):55, aug 2015. ISSN 1538-4357. doi: 10.1088/0004-637X/809/1/55. URL http://stacks.iop.org/0004-637X/809/i=1/a=55?key=crossref.31615a3684cb806f66f67b3c2b7d1789.

C. K. Birdsall and A. B. Langdon. *Plasma Physics via Computer Simulation*. McGraw-Hill, Electrical Engineering and Computer Sciences Department, University of California, Berkeley, 1991.

Johannes Brandstetter, Daniel Worrall, and Max Welling. Message passing neural pde solvers. *arXiv preprint arXiv:2202.03376*, 2022.

B.I. Cohen, A.J. Kemp, and L. Divol. Simulation of laser-plasma interactions and fast-electron transport in inhomogeneous plasma. *J. Comput. Phys.*, 229(12):4591–4612, jun 2010. ISSN 0021-9991.

John M. Dawson. Particle simulation of plasmas. *Rev. Mod. Phys.*, 55:403–447, Apr 1983. doi: 10.1103/RevModPhys.55.403. URL https://link.aps.org/doi/10.1103/RevModPhys.55.403.

F. Fiuza, M. Marti, R. A. Fonseca, L. O. Silva, J. Tonge, J. May, and W. B. Mori. Efficient modeling of laser-plasma interactions in high energy density scenarios. *Plasma Physics and Controlled Fusion*, 53(7):74004–74015, jul 2011. ISSN 07413335. doi: 10.1088/0741-3335/53/7/074004. URL https://iopscience.iop.org/article/10.1088/0741-3335/53/7/074004https://iopscience.iop.org/article/10.1088/0741-3335/53/7/074004/meta.

S. E. Guidoni, C. R. DeVore, J. T. Karpen, and B. J. Lynch. Magnetic-island contraction and particle acceleration in simulated eruptive solar flares. *The Astrophysical Journal*, 820(1):60, 2016. doi: 10.3847/0004-637x/820/1/60. URL https://doi.org/10.3847%2F0004-637x%2F820%2F1%2F60.

Diederik P Kingma and Jimmy Ba. Adam: A method for stochastic optimization. *arXiv preprint arXiv:1412.6980*, 2014.

Yu. L. Klimontovich. *The Statistical Theory of Non-Equilibrium Processes in a Plasma*. MIT Press, Cambridge, 1967.

Dmitrii Kochkov, Jamie A Smith, Ayya Alieva, Qing Wang, Michael P Brenner, and Stephan Hoyer. Machine learning–accelerated computational fluid dynamics. *Proceedings of the National Academy of Sciences*, 118(21), 2021.

G. Kowal, E. M. de Gouveia Dal Pino, and A. Lazarian. Magnetohydrodynamic simulations of reconnection and particle acceleration: three-dimensional effects. *The Astrophysical Journal*, 735(2):102, 2011. doi: 10.1088/0004-637x/735/2/102. URL https://doi.org/10.1088%2F0004-637x%2F735%2F2%2F102.

Florian Kroll, Florian-Emanuel Brack, Constantin Bernert, Stefan Bock, Elisabeth Bodenstein, Kerstin Brüchner, Thomas E. Cowan, Lennart Gaus, René Gebhardt, Uwe Helbig, Leonhard Karsch, Thomas Kluge, Stephan Kraft, Mechthild Krause, Elisabeth Lessmann, Umar Masood, Sebastian Meister, Josefine Metzkes-Ng, Alexej Nossula, Jörg Pawelke, Jens Pietzsch, Thomas Püschel, Marvin Reimold, Martin Rehwald, Christian Richter, Hans-Peter Schlenvoigt, Ulrich Schramm, Marvin E. P. Umlandt, Tim Ziegler, Karl Zeil, and Elke Beyreuther. Tumour irradiation in mice with a laser-accelerated proton beam. *Nature Physics*, 18(3):316–322, mar 2022. ISSN 1745-2481. doi: 10.1038/s41567-022-01520-3. URL https://www.nature.com/articles/s41567-022-01520-3.

Zongyi Li, Nikola Borislavov Kovachki, Kamyar Azizzadenesheli, Burigede liu, Kaushik Bhattacharya, Andrew Stuart, and Anima Anandkumar. Fourier neural operator for parametric partial differential equations. In *International Conference on Learning Representations*, 2021. URL https://openreview.net/forum?id=c8P9NQVtmnO.

Ilya Loshchilov and Frank Hutter. Sgdr: Stochastic gradient descent with warm restarts. *arXiv preprint arXiv:1608.03983*, 2016.

P. Patel, A. Mackinnon, M. Key, T. Cowan, M. Foord, M. Allen, D. Price, H. Ruhl, P. Springer, and R. Stephens. Isochoric heating of solid-density matter with an ultrafast proton beam. *Physical Review Letters*, 91(12):125004, 9 2003. ISSN 0031-9007. doi: 10.1103/PhysRevLett.91.125004. URL https://link.aps.org/doi/10.1103/PhysRevLett.91.125004.

J. R. Rygg, F. H. Séguin, C. K. Li, J. A. Frenje, M. J.-E. Manuel, R. D. Petrasso, R. Betti, J. A. Delettrez, O. V. Gotchev, J. P. Knauer, D. D. Meyerhofer, F. J. Marshall, C. Stoeckl, and W. Theobald. Proton radiography of inertial fusion implosions. *Science*, 319(5867):1223–5, 2 2008. ISSN 1095-9203. doi: 10.1126/science.1152640. URL http://www.ncbi.nlm.nih.gov/pubmed/18309079.

Alvaro Sanchez-Gonzalez, Jonathan Godwin, Tobias Pfaff, Rex Ying, Jure Leskovec, and Peter Battaglia. Learning to simulate complex physics with graph networks. In *International Conference on Machine Learning*, pp. 8459–8468. PMLR, 2020.

T.E. Schwartzentruber and I.D. Boyd. A hybrid particle-continuum method applied to shock waves. *Journal of Computational Physics*, 215(2):402–416, 2006. ISSN 0021-9991. doi: https://doi.org/10.1016/j.jcp.2005.10.023. URL https://www.sciencedirect.com/science/article/pii/S0021999105004936.

R. A. Snavely, M. H. Key, S. P. Hatchett, T. E. Cowan, M. Roth, T. W. Phillips, M. A. Stoyer, E. A. Henry, T. C. Sangster, M. S. Singh, S. C. Wilks, A. MacKinnon, A. Offenberger, D. M. Pennington, K. Yasuike, A. B. Langdon, B. F. Lasinski, J. Johnson, M. D. Perry, and E. M. Campbell. Intense high-energy proton beams from petawatt-laser irradiation of solids. *Phys. Rev. Lett.*, 85(14):2945–2948, 10 2000. doi: 10.1103/PhysRevLett.85.2945. URL https://link.aps.org/doi/10.1103/PhysRevLett.85.2945.

Meng Tang, Yimin Liu, and Louis J Durlofsky. A deep-learning-based surrogate model for data assimilation in dynamic subsurface flow problems. *Journal of Computational Physics*, 413:109456, 2020.

Kiwon Um, Robert Brand, Yun Raymond Fei, Philipp Holl, and Nils Thuerey. Solver-in-the-loop: Learning from differentiable physics to interact with iterative pde-solvers. *Advances in Neural Information Processing Systems*, 33:6111–6122, 2020.

Pantelis R Vlachas, Georgios Arampatzis, Caroline Uhler, and Petros Koumoutsakos. Multiscale simulations of complex systems by learning their effective dynamics. *Nature Machine Intelligence*, 4(4):359–366, 2022.

S. C. Wilks, A. B. Langdon, T. E. Cowan, M. Roth, M. Singh, S. Hatchett, M. H. Key, D. Pennington, A. MacKinnon, and R. A. Snavely. Energetic proton generation in ultra-intense laser–solid interactions. *Physics of Plasmas*, 8(2):542–549, 2001. doi: 10.1063/1.1333697. URL https://doi.org/10.1063/1.1333697.

Tailin Wu, Takashi Maruyama, and Jure Leskovec. Learning to accelerate partial differential equations via latent global evolution. *arXiv preprint arXiv:2206.07681*, 2022a.

Tailin Wu, Qinchen Wang, Yinan Zhang, Rex Ying, Kaidi Cao, Rok Sosič, Ridwan Jalali, Hassan Hamam, Marko Maucec, and Jure Leskovec. Learning large-scale subsurface simulations with a hybrid graph network simulator. *Proceedings of the 28th ACM SIGKDD Conference on Knowledge Discovery and Data Mining (KDD '22)*, 2022b.